Metallic transport properties of amorphous nickel–silicon films

R Rosenbaum†, A Heines†, A Palevski†, M Karpovski†, A Gladkikh†, M Pilosof†, A J Daneshvar‡, M R Graham‡, T Wright‡, J T Nicholls‡, C J Adkins‡, M Witcomb§, V Prozesky‖, W Przybylowicz‖ and R Pretorius‖

† Tel Aviv University, School of Physics and Astronomy, Raymond and Beverly Sackler Faculty of Exact Sciences, Ramat Aviv, 69978, Israel
‡ Cavendish Laboratory, Madingley Road, Cambridge CB3 0HE, UK
§ University of the Witwatersrand, Electron Microscope Unit, Private Bag 3, Wits, 2050, South Africa
‖ National Accelerator Centre, Van de Graaff Group, PO Box 72, Faure 7131, South Africa

Abstract. Transport properties including conductivity and magnetoconductance have been measured for amorphous nickel–silicon films. This study focuses on metallic amorphous a-Ni$_x$Si$_{1-x}$ films, located just above the metal–insulator transition (MIT). Using various techniques, the MIT was identified. Electron–electron interactions dominated the conductivity, where $\sigma \approx \sigma(0) + CT^{0.55}$. Strong spin–orbit scattering was important in the weak-localization contribution to the magnetoconductance data for the metallic films. The inelastic scattering time was extracted from the magnetoconductance data. The low-temperature magnetoconductance data versus Ni content x exhibited a negative maximum just above the critical concentration x_c, suggesting another technique for identifying the MIT.

1. Introduction

Amorphous nickel–silicon is a good system in which to study the effects of electron–electron interactions upon the transport properties. The electronic transport in this system appears not to be complicated by percolation and granular effects and probably not by superconductivity.

Limited studies have been made on the nickel–silicon systems. The *amorphous* nickel–silicon alloy, a-Ni$_x$Si$_{1-x}$, has been investigated by the groups of Adkins, of Davis, and of Belu-Marian [1, 2]. Dammer *et al* reported that 1 μm thick films were metallic at $x = 0.22$ (22 at.% Ni) and insulating at $x = 0.15$ [1]. No films were studied in the close vicinity of the metal–insulator transition (MIT), and the critical metallic Ni concentration x_c was estimated to be approximately $x_c \approx 0.18$ [1]. At liquid helium temperatures, Dammer *et al* observed negative magnetoconductance (MC) values only, for both the metallic and the insulating films [1]. The MC data were not directly compared to the 3D theories, but the negative sign of the MC was attributed to electron–electron interactions [1]. Hall measurements were made, yielding a carrier density of approximately 9×10^{27} m^{-3} [1]. Belu-Marian *et al* have made structure, optical, and conductivity studies of amorphous Ni$_x$Si$_{1-x}$ films [2].

Abkemeier *et al* have studied hydrogenated amorphous nickel–silicon alloys, and have estimated the MIT to be at $x = 0.24$ to 0.25 [3, 4]. Hydrogen 'passivates' dangling bonds

of the amorphous Si and saturates them. In unsaturated samples, the dangling bonds donate electrons to the nickel bands. Thus, in *hydrogenated* samples, a higher Ni concentration would be required to effect a MIT.

Collver has studied the *crystalline* metastable nickel–silicon system around the MIT, and reported a critical metal content of 0.13 for c-Ni_xSi_{1-x} [5, 6]. Resistivity and magnetoresistance studies have been made by Belu-Marian's group [7, 8].

This paper summarizes electrical conductivity data taken over a wide temperature range and magnetoconductance data taken at liquid helium temperatures and below for *amorphous* Ni_xSi_{1-x}. The measurements were made on metallic films located just above the MIT. Using 3D transport theories, reasonable magnitudes for the fitting parameters are reported for the metallic films. Several methods are presented for determining the location of the MIT. The properties of the insulating films are summarized in another paper [9].

2. Film fabrication and characterization

Thin amorphous nickel–silicon a-Ni_xSi_{1-x} films were prepared by co-evaporating Ni and Si using two electron guns. Seven to eight narrow glass pieces of 2.5 mm width were glued onto a microscope glass slide. These narrow glass segments were employed to avoid shadowing problems which are introduced when using a mask. Three microscope glass slides were placed 'end to end' above and between the Ni and Si graphite boats in order to obtain differences in the Ni content. Small broken glass fragments coated with photoresist were placed between the glued glass pieces, so that EDAX (energy-dispersive analysis of x-rays) samples would also be available. Typical evaporation rates were 1.4 Å s^{-1} and 7 Å s^{-1} for the Ni and Si sources. The evaporations were performed in vacua of 10^{-6} mm Hg, and the glass slices were held at room temperature. The Ni had a purity of 99.9% and the Si had a purity of 99.97%. As a check against contamination, the original graphite boats were replaced with new boats containing new charges of materials; the resulting new series of films nicely reproduced the transport results of the original series. None of the series show superconducting properties, which could possibly arise from boat contamination, particularly with Cu [10].

Film homogeneity is very important near the MIT. We had experienced great difficulty in stabilizing the Si evaporation rate, resulting in very inhomogeneous films. However, we noticed that the Si evaporation rate would generally stabilize to a steady value if the Si boat was heated for at least ten minutes. Quartz crystal monitors, positioned above each graphite boat, monitored the evaporation rates and hence the thicknesses of the Ni and Si deposited films during the evaporation. The Ni and Si thicknesses were simultaneously read every ten seconds during the evaporation. The Ni thickness was then plotted versus the Si thickness; any deviations from a straight line indicated instability in the evaporation rate of one of the two materials. Thus, any series that exhibited deviations from a straight-line fit was considered to be inhomogeneous and was discarded. Some ten evaporations were attempted before a straight line was obtained, as illustrated in figure 1 for the No 300 series. We believe that this series is homogeneous to better than ±2.5% throughout the typical thickness of 1100 Å.

The following procedure was used for the samples studied in the transmission electron microscope (TEM). Thin 1100 Å a-Ni_xSi_{1-x} films were deposited onto photoresist-coated glass slide fragments located between the sample slices; these thin films were lifted off from the glass fragments using acetone, and floated onto fine copper grids, which were used for mechanically supporting the fragile films in the TEM. Dark-field micrographs from the TEM showed no structure but only a sandy background, demonstrating the amorphous
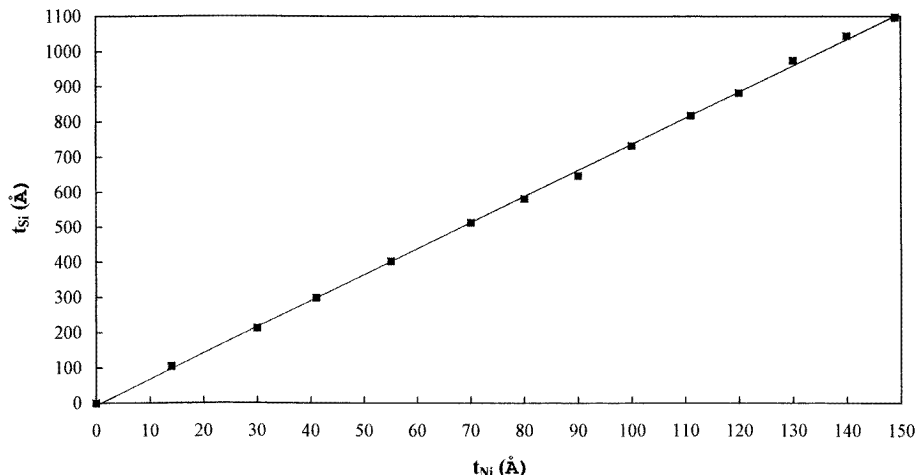
Figure 1. The thickness measured by the Si thickness monitor versus the thickness measured by the Ni thickness monitor during the evaporation of the a:Ni$_x$Si$_{1-x}$ No 300 series. A deviation from a straight line indicates variations in the evaporation rate of one of the two heated sources, and hence inhomogeneities in the films. The films in this series are homogeneous to better than ±2.5% throughout their thicknesses.

nature of the samples. Broad Ni and Si diffraction rings were observed, characteristic of the amorphous structure.

EDAX of the Ni and Si contents was performed using a Link AN10000 EDS system attached to a JSM-840 SEM. Each film was supported on a copper grid. The x-ray spectra were collected from nine or ten different regions along the length of each film, each region being of area 0.01 mm^2. The analyses were carried out at 4.13 kV in order to contain all of the analysis volume within the film. There was no change to the analysis result whether an electrically grounded single-layer film or double-folded film was analysed over or between the underlying supporting grid bars of the 300-mesh copper grid. The film was positioned over the centre of the hole in a Faraday cage made out of spectrographically pure carbon in order to prevent any forward-scattered x-rays being deflected back towards the EDS detector. The x-ray data were quantified using a bulk correction routine (ZAF-4/FLS) using pure element standards. The compositional spread about the averaged value of both elements for all films was estimated to be ±0.4 at.%.

Typical atomic Ni fractions for the films are given in table 1, as well as the thicknesses *t* and room temperature conductivities σ_{RT}.

Notice in table 1 that, for films having large Ni contents, there are significant variations in the room temperature conductivities, σ_{RT}. These variations were first noticed by Bela-Marian's group and were attributed to the formation of the polycrystalline NiSi$_2$ silicide [2].

Microprobe Rutherford backscattering (RBS) and photo-induced x-ray emission (PIXE) measurements were performed at the National Accelerator Centre in South Africa. The nickel content of 25 at.% for film No 18 was reconfirmed by the group who performed these measurements. Moreover, this group observed non-uniformity in the film thicknesses ranging by a factor of two or more for different regions in each film.

Film No 18 is located just above the MIT. From the EDAX results, the critical metallic concentration x_c is 24.8%; this value is rather high. There is a remote possibility that some of the silicon bonds have been passivated with hydrogen. Although no hydrogen was

Table 1. Atomic percentages, thicknesses, and room temperature conductivities for the films.

Film No	x (at.% Ni, EDAX)	t (Å)	σ_{RT} (Ω^{-1} cm^{-1})
19	23.5	1230	116
18	24.8	1220	163
17	26.4	1200	186
16	28.2	1180	278
15	30.0	1155	299
14	31.9	1125	364
13	33.7	1095	448
12	35.6	1055	532
11	37.4	1015	657
10	39.3	975	724
9	41.1	930	691
8	42.9	890	794
7	44.8	865	1015
6	46.7	843	967

introduced during the evaporation, Gerd Bergmann pointed out to us the possibility that the electron beams can produce atomic hydrogen by 'cracking' the diffusion pump oil that has slowly back-steamed into the evaporation chamber during the long evacuation time [11].

On the basis of RBS data, Arnulf Möbius has suggested alternative values for the nickel content [12]. The reasons for the discrepancies between the RBS and EDAX values are not currently understood.

Indium tabs were pressed onto the films as electrical contacts. Measurements were made in a ^{3}He refrigerator and/or a ^{4}He cryostat, both equipped with 4 T magnets.

3. Low-temperature conductivity data and the metal–insulator transition

Films may be classified electronically as being either insulating or metallic. Insulating 3D films exhibit infinite resistivity or zero conductivity at the absolute zero temperature. In contrast, metallic 3D films always display a finite resistivity or non-zero positive conductivity at absolute zero.

The conductivities for a:Ni$_x$Si$_{1-x}$ films spanning the MIT are shown in figure 2. Films No 23 and No 22 are easy to identify as insulating films since their conductivities tend towards zero at low temperatures. In contrast, the conductivity of film No 16 appears to tend to finite values at absolute zero as seen in figure 2, and this film is most probably metallic. The conductivities of the other films show no discontinuous jumps as the MIT is crossed. It is not obvious whether film No 19 and its neighbouring films, film No 18 and film No 20, are located below the MIT on the insulating side or are located above the MIT on the metallic side. This paper describes several techniques for locating the MIT.

Strongly insulating films exhibit an activated hopping conductivity which can be described by the variable-range hopping (VRH) expression

$$\sigma(T) = \sigma_0[\exp -(T_0/T)^y] \tag{1}$$

where σ_0 is the prefactor, T_0 is a characteristic temperature, and y is an exponent.

In contrast, the conductivity of a *3D metallic* film at sufficiently low temperatures can be described by the power-law expression

$$\sigma(T) = \sigma(0) + CT^z \tag{2}$$
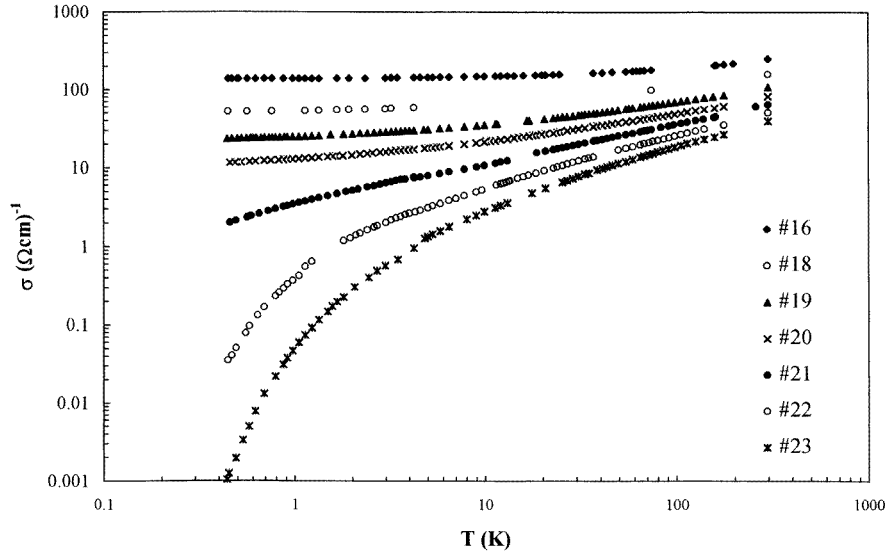
Figure 2. Zero-field conductivities versus temperature for different a-Ni$_x$Si$_{1-x}$ films. It is not obvious from simple inspection of this plot where the MIT is located.

where $\sigma(0)$ is the positive zero-temperature conductivity, C is the prefactor, and z is the exponent of the temperature power law. Equation (2) might approximate the conductivity contribution from the 3D electron–electron interaction theory and/or from the 3D weak-localization theory. We will investigate the validity of equation (2) and determine the magnitudes of its fitting parameters. Note that in the above procedures, y and z are free fitting parameters. We will later refer to equation (2) as the 'empirical fit' to the data.

A useful technique for identifying the MIT was previously introduced [13, 14]. The mathematical function $w(T)$ exhibits distinctively different temperature behaviours for insulating and metallic films:

$$w(T) = \mathrm{d}\ln\sigma/\mathrm{d}\ln T = (T/\sigma)\ \mathrm{d}\sigma/\mathrm{d}T. \tag{3}$$

In practice, the w's are calculated from two conductivity points, $\sigma_1(T_1)$ and $\sigma_2(T_2)$, closely separated by the temperatures T_1 and T_2, using one of the following expressions:

$$w(T_{ave}) \approx (\ln\sigma_1 - \ln\sigma_2)/(\ln T_1 - \ln T_2) \tag{4a}$$

and the approximation

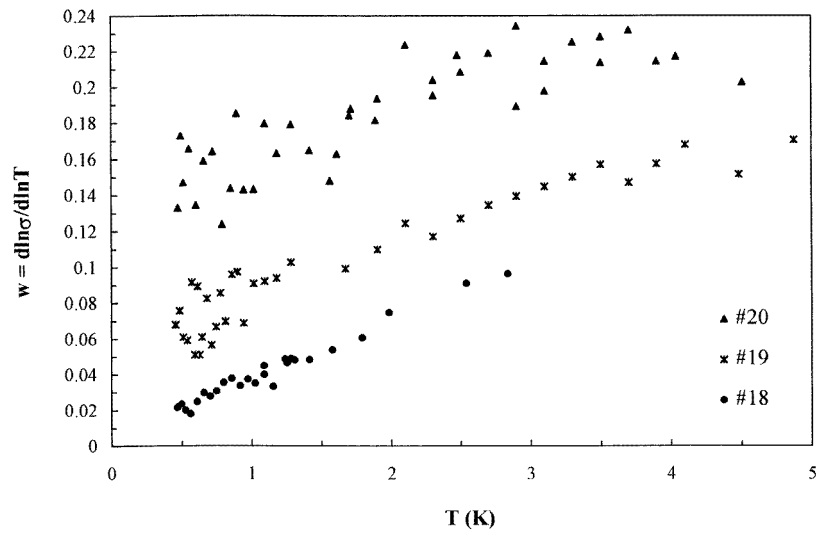$$w(T_{ave}) \approx T_{ave}(\ln\sigma_1 - \ln\sigma_2)/(T_1 - T_2) \tag{4b}$$

where

$$T_{ave} = (T_1 + T_2)/2.$$

For strongly insulating films exhibiting VRH conductivity, inserting equation (1) into equation (3) yields

$$w(T) = y(T_0/T)^y. \tag{5}$$

Notice that $w(T)$ *increases* to infinity as the temperature approaches absolute zero.

Figure 3. A plot of $w = \mathrm{d}\ln\sigma/\mathrm{d}\ln T$ versus temperature for films No 20, No 19, and No 18. The decreasing behaviour of $w(T)$ towards *zero* with decreasing temperature identifies film No 18 as a *metallic* film. In contrast, the *finite* extrapolated value for w as $T \to 0$ for both films No 20 and No 19 identifies each of these films as an *insulating* film.

Conductivity and Empirical Fit Vs. Low Temperatures for Film #18
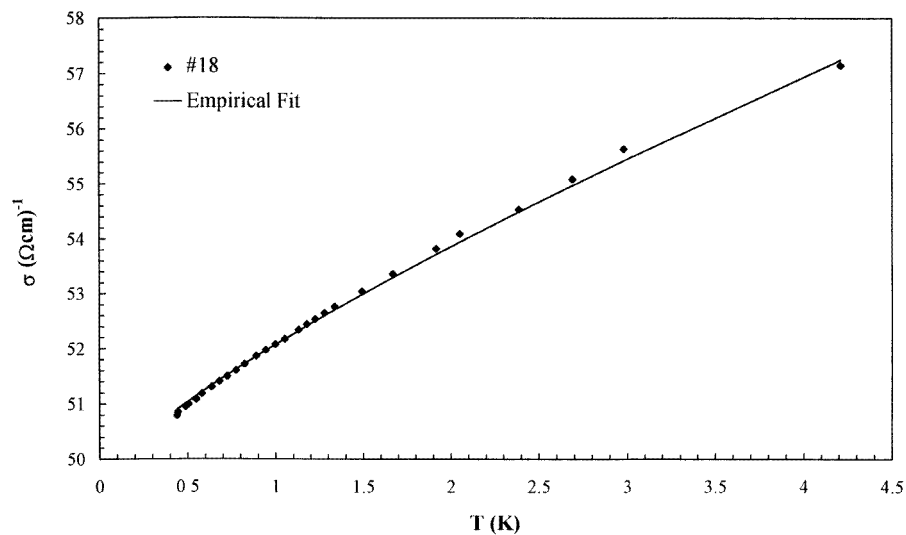
Figure 4. Low-temperature, zero-field conductivity data versus temperature for the metallic film No 18. The solid line is an empirical fit made using $\sigma(T) = 49.6 + 2.46T^{0.79}$ in Ω^{-1} cm^{-1}.

For 3D *metallic films* exhibiting slowly decreasing conductivities with decreasing

temperatures at low temperatures, equation (2) can be substituted into equation (3) to yield

$$w(T) = zCT^z/[\sigma(0) + CT^z] = zCT^z/\sigma(T). \qquad (6)$$

Observe that if the film is indeed *metallic* and exhibits a finite positive conductivity $\sigma(0)$ at absolute zero, then $w(T)$ should extrapolate to zero at absolute zero. An example of metallic behaviour is shown in figure 3 where film No 18 exhibits w's which tend to zero as $T \to 0$ K. For this metallic case, a least-regression fit of the $\log(w\sigma)$ versus $\log T$ data yields values for the exponent z and the prefactor C according to equation (6). A value for $\sigma(0)$ follows directly from one of the data points. The empirical fit to the zero-field low-temperature conductivity data for film No 18 below 4 K is shown in figure 4 where the solid line is given by $\sigma(T) = 49.6 + 2.46T^{0.79}$ in Ω^{-1} cm^{-1}. In contrast, the w-behaviours exhibited by films No 19 and No 20 suggest that the w's extrapolate to *finite values* and not to zero as seen in figure 3. Hence, these two films are insulating and are located slightly below the MIT.

The fitting parameters obtained by using equation (2) are summarized in table 2 for the metallic films.

Table 2. Fitting parameters for the metallic conductivity empirical expression, equation (2).

Film No	Exponent z	C (Ω^{-1} cm^{-1} (K^z)$^{-1}$)	$\sigma(0)$ (Ω^{-1} cm^{-1})	Temperature range
18	0.79	2.46	49.6	0.45 K to 4.2 K
17	0.68	2.81	68.4	0.45 K to 4.2 K
16	0.53	3.98	136	0.45 K to 16 K
15	0.57	3.48	169	0.45 K to 4.2 K
14	0.60	3.56	221	0.45 K to 4.2 K
13	0.36	8.06	289	1.3 K to 4.2 K
12	0.34	7.58	362	1.3 K to 4.2 K
11	Forced 1/2	5.65	472	1.4 K to 4.2 K
10	Forced 1/2	6.85	552	1.3 K to 4.2 K

The surprising result from table 2 is the average value of 0.55 for the exponent z of the power-law temperature term, which is rather close to the value of 1/2 predicted from the 3D electron–electron interaction theory to be discussed later. We have observed in other systems values for z that are either considerably greater or considerably smaller than 1/2; for example granular AlGe films exhibit z-values close to 0.1 [14] and 'normal' AlGe films have z-values close to 1.2 [15].

Another method for determining the critical metallic content x_c is based upon the scaling theory that predicts the continuous MIT in a 3D disordered system [16] in contrast to the concept of a minimum metallic conductivity given by Mott [17]. The zero-temperature conductivity can be extrapolated to zero according to $\sigma(0) = \sigma_0(x - x_c)^s$. For our case of strong spin–orbit scattering, the effective critical conductivity exponent s is predicted to be $s \approx 1$, associated with the spin–orbit universality class [18–20]. Belitz has emphasized that the extrapolation is valid only in the critical region—that is, when x takes on values that are less than 10% of x_c [21, 18]. We have only two films that meet this requirement, namely films No 18 and No 17; thus, an extrapolation in the critical region is not meaningful [21]. If we extend the extrapolation outside the critical region to include all of the values of $\sigma(0)$ appearing in table 2, then the critical concentration is found to be located between those of films No 19 and No 18, regardless of whether the RBS or EDAX values are used for x [12]. This result is consistent with the w-prediction.

Shlimak *et al* have recently proposed an alternative method for determining values for $\sigma(0)$ where $\sigma(0) \approx \sigma_x(T^*) - \sigma_{xc}(T^*)$ [22]. In their scheme, $\sigma_{xc}(T^*)$ is the conductivity of the film located just at the MIT and evaluated at a fixed experimental low temperature T^*. Choosing $T^* = 1.49$ K, and choosing the conductivity of film No 18 for σ_{xc}, we obtained values for $\sigma(0)$ as a function of x for the remaining films. These values of $\sigma(0)$ were considerably smaller, by 50% to 20%, than those obtained from the empirical fit technique. It is not clear what the reason is for this discrepancy.

An upper limit on the Mott minimum conductivity can be estimated. Since film No 18 is the film closest to the MIT that is definitely metallic, the Mott minimum conductivity σ_{Mott} must be less than this film's conductivity at low temperatures. Film No 18 has a conductivity of 51 Ω^{-1} cm^{-1} at $T = 0.5$ K, which is considerably less than the 180 Ω^{-1} cm^{-1} estimation according to $\sigma_{\text{Mott}} \approx 0.03e^2/\hbar a$ [17]; here, a is the impurity separation distance taken to be 4 Å. Perhaps the prefactor of 0.03 is incorrect.
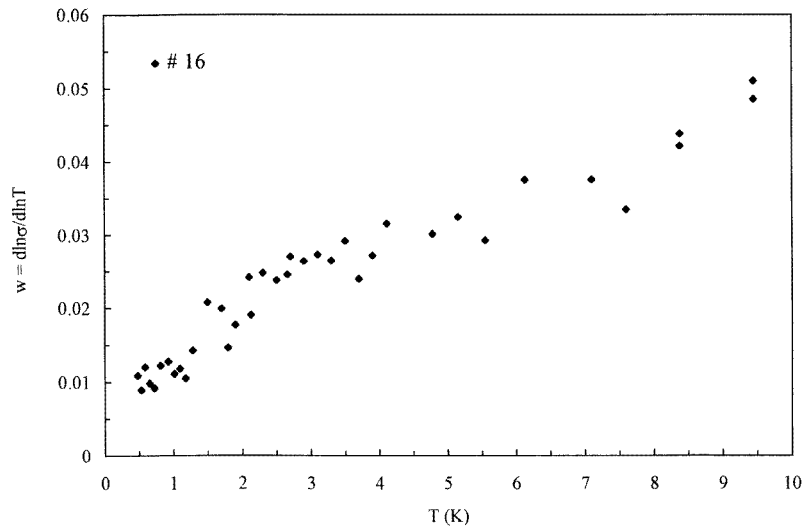

Figure 5. A plot of $w(T) = \mathrm{d}\ln\sigma/\mathrm{d}\ln T$ versus temperature for film No 16. The decreasing of $w(T)$ towards *zero* with decreasing temperatures identifies this film as a *metallic* film.

4. Low-temperature magnetoconductance and zero-field conductivity data

The low-temperature MC data yield values for the inelastic scattering time $\tau_{in}(T)$ and insight into the processes that drive the films insulating. Film No 16, the third film located above the MIT, was studied. It exhibits w-values which tend to extrapolate to zero as $T \rightarrow 0$, as shown in figure 5. Its conductivity can be well fitted by the empirical expression $\sigma(T) = 136 + 3.98T^{0.53}$ in Ω^{-1} cm^{-1}, illustrated in figure 6. The second term agrees well with the electron–electron interaction (EEI) theory prediction.

The low-temperature MC data, $\Delta\sigma = \sigma(B) - \sigma(0)$, for the metallic film No 16 are shown in figure 7. Notice that the MC data are negative except for an anomalous positive behaviour for magnetic fields smaller than 0.4 T as seen in figure 7. The negative $B^{1/2}$-behaviour of the MC data at large fields strongly suggests contributions from the 3D weak-localization (WL) theory involving strong spin–orbit scattering, and from the 3D EEI theory. For the 3D
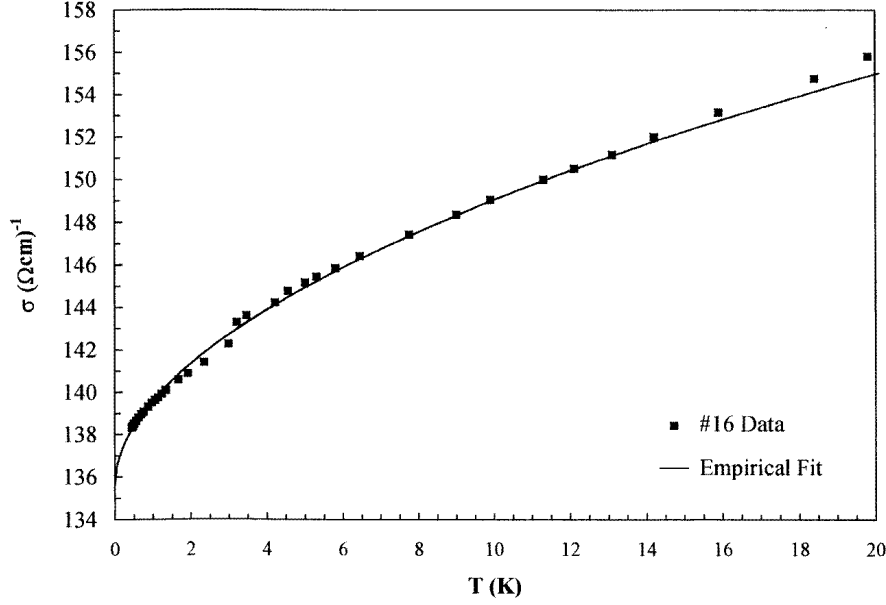
Figure 6. Low-temperature, zero-field conductivity data versus temperature for the metallic film No 16. The $T^{0.53}$-dependence of $\sigma(T)$ suggests that EEI dominate the conduction process; details of the empirical fitting procedure, represented by the solid line, are described in the text.

theories to be valid, the thermal length $L_T = (D_{dif}\hbar/k_BT)^{1/2}$ must be considerably smaller than the film thickness of 1100 Å; and the inelastic length $L_{in} = [D_{dif}\tau_{in}(T)]^{1/2}$ should also be considerably less than the film thickness. The condition for three dimensionality is satisfied provided that the diffusion constant D_{dif} is less than 1 cm^2 s^{-1}. It is predicted by Entin-Wohlman *et al* [23] that just above the MIT, that $D_{dif} = D_0(x - x_c)^{t-\beta}$ where t is the conductivity exponent, equal to 1.9 in 3D [24] and to 1.3 in 2D [25], and β is the finite-cluster mass exponent, equal to 0.41 [26]. Since $D_0 \approx 50$ cm^2 s^{-1} for a very metallic film, the diffusion constant is estimated to take on values less than 1 cm^2 s^{-1} near the MIT.

EEI produce a dip in the density of states about E_F. This dip results in a small correction to the zero-field conductivity that reduces the conductivity with decreasing temperatures. According to the 3D prediction of Altshuler and Aronov [27], the particle–hole contribution arising from EEI to the zero-field conductivity is

$$\sigma_{EEI}(T) = \frac{1.294}{\sqrt{2}} \frac{e^2}{4\pi^2\hbar} \left(\frac{4}{3} - \frac{3}{2}\tilde{F}_\sigma \right) \left(\frac{k_BT}{\hbar D_{dif}} \right)^{1/2} \tag{7}$$

where the electron screening parameter $\tilde{F}_\sigma$ ranges between 0.2 to 0.4 for many thin metallic films. Notice that the $T^{1/2}$-dependence is in reasonable agreement with the temperature power term determined by using equation (2), as shown in table 2. The predicted $T^{1/2}$-behaviour might be expected to change to $T^{1/3}$ just above the MIT [28], but this is not observed in these films.

Lee and Ramakrishnan have calculated the 3D MC contribution arising from EEI in the particle–hole channel [29]:

$$\Delta\sigma_{EEI}(B,T) = \frac{-e^2}{4\pi^2\hbar} \tilde{F}_\sigma \left(\frac{k_BT}{2\hbar D_{dif}} \right)^{1/2} g_3\left(\frac{g_e\mu_B B}{k_BT} \right) \tag{8}$$

B (T)
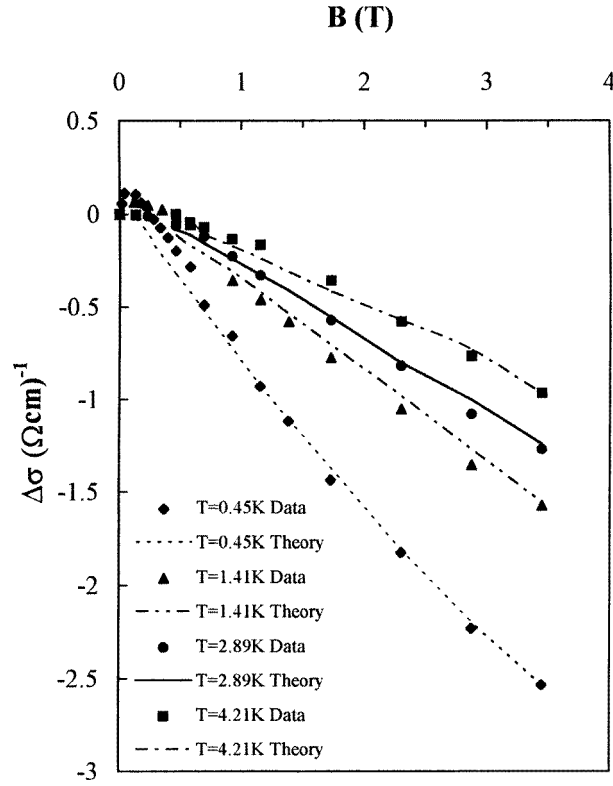
Figure 7. MC data for the metallic film No 16 versus magnetic field. Above $B = 1$ T, the MC data follow a $B^{1/2}$-dependence. The 3D WL and EEI theories made important contributions to the theoretical fits. The spin–orbit scattering is strong. The lines are fits made using equations (8) and (11).

where g_e is the Landé factor. For bulk Si, Feher has observed that g_e is slightly less than 2 [30], and Roth has confirmed the experimental results theoretically [31]. The function g_3 is very sensitive to the argument $g_e \mu_B B / k_B T$. We have taken g_e for amorphous Si to be 2, although the best fits are given when $g_e \approx 1.8$. Ousset *et al* have suggested suitable approximations for the function $g_3(x)$ [32]:

$$g_3(x) \approx 5.6464 \times 10^{-2} x^2 - 1.4759 \times 10^{-3} x^4 + 4.2747 \times 10^{-5} x^6$$
$$- 1.5351 \times 10^{-6} x^8 + 6 \times 10^{-8} x^{10} \qquad x \leqslant 3 \qquad (9a)$$

$$g_3(x) \approx 0.645\,48 + 0.235(x - 4) - 7.45 \times 10^{-4}(x - 4)^2 - 2.94 \times 10^{-3}(x - 4)^3$$
$$+ 6.32 \times 10^{-4}(x - 4)^4 - 5.22 \times 10^{-5}(x - 4)^5 \qquad 3 \leqslant x \leqslant 8 \qquad (9b)$$

and

$$g_3(x) \approx x^{1/2} - 1.2942 - \frac{\pi^2}{12x^{3/2}} - \frac{\pi^4}{16x^{7/2}} - \frac{5\pi^6}{32x^{11/2}} \qquad x \geqslant 8. \qquad (9c)$$

The limiting forms of g_3 for large and small x are

$$g_3(x \to \infty) \approx \sqrt{x} - 1.29 \qquad \text{and} \qquad g_3(x \to 0) \approx 0.0565x^2. \qquad (9d)$$

Note that the high-field behaviour of $\Delta\sigma_{EEI}$ has the $B^{1/2}$-dependence observed in the MC data. It is useful to note that $g_e \mu_B / k_B \approx 4/3$ in units of K T^{-1} if $g_e = 2$.

Owing to the lack of any other better formalism, we use the 3D WL theory close to the MIT for film No 16; the WL theory generally applies to very metallic films. Kawabata first derived the 3D WL correction to the zero-field conductivity for the case of no spin–orbit scattering [33]. Fukuyama and Hoshino extended the Kawabata results to include the spin–orbit scattering τ_{so} and obtained a zero-field correction to the conductivity [34]; Hickey *et al* have suggested the following expression that includes magnetic spin scattering [35]:

$$\sigma_{WL}(T) = \frac{e^2}{2\pi^2\hbar} \frac{1}{\sqrt{D_{dif}}} \left[3\left(\frac{1}{4\tau_{in}(T)} + \frac{1}{3\tau_{so}} + \frac{1}{\tau_s} \right)^{1/2} - \left(\frac{1}{4\tau_{in}(T)} + \frac{1}{4\tau_s} \right)^{1/2} \right] \qquad (10)$$

where τ_{so} is the temperature-independent spin–orbit scattering time, τ_s is the temperature-independent magnetic spin scattering time, and $\tau_{in}(T/\text{K})$ is the temperature-dependent inelastic scattering time. It should be noted that a number of different conventions are used in the definition of τ_{so}. The one followed here in equation (10) is that adopted by Bergmann and by Baxter *et al* [36, 37]. When comparing with results of other authors, it might be necessary to redefine τ_{so} as $\tau_{so}/3$. A magnitude for the spin–orbit scattering time [38, 39] can be estimated from the expression $\tau_{so} \approx \tau_0(137/Z)^4$ where Z is the atomic number ($Z = 28$ for Ni) and where $\tau_0 \approx 10^{-15}$ s is the elastic scattering time. For the case of weak spin–orbit scattering when τ_{so} is large, equation (10) predicts that $\sigma_{WL} \propto (\tau_{in})^{-1/2}$; this is the case of WL that causes a decrease of the conductivity with decreasing temperatures. For our case of strong spin–orbit scattering and a small magnitude for τ_{so}, equation (10) predicts weak anti-localization where $\sigma_{WL} \propto (-1/2)(\tau_{in})^{-1/2}$; in this case, the WL contribution produces an *increase* in the conductivity with decreasing temperature, in opposition to the EEI contribution. However, the EEI contribution seems always to dominate, resulting in an overall major decrease of the conductivity with decreasing temperature.

The 3D WL MC expression was suggested by Baxter *et al* [37], who extended the results of Fukuyama and Hoshino [34] to include weak magnetic scattering such that $\tau_s \gg \tau_{so}$:

$$\Delta\sigma_{WL}(B, T) = \frac{e^2}{2\pi^2\hbar} \sqrt{\frac{eB}{\hbar}} \left[\frac{3}{2} f_3\left(\frac{B}{B_{in}(T) + \frac{4}{3}B_{so} + \frac{2}{3}B_s} \right) - \frac{1}{2} f_3\left(\frac{B}{B_{in}(T) + 2B_s} \right) \right] \qquad (11)$$

where $B_x = \hbar/(4eD_{dif}\tau_x)$. The Zeeman splitting correction at high fields has been neglected [34, 37]. Baxter *et al* gave a numerically convenient approximation for the function $f_3(x)$, which is accurate over the entire range of x, and retains the correct asymptotic limits [37]:

$$f_3(x) \approx 2\sqrt{2 + 1/x} - 2\sqrt{1/x} - \frac{1}{\sqrt{1/2 + 1/x}} - \frac{1}{\sqrt{3/2 + 1/x}} + \frac{1}{48}(2.03 + 1/x)^{-3/2}$$

$$(12a)$$

$$f_3(x \to \infty) \to \frac{x^{3/2}}{48} \qquad (12b)$$

and

$$f_3(x \to \infty) \to 0.6049. \qquad (12c)$$

Note that $\Delta\sigma_{WL}$ exhibits a $B^{1/2}$-dependence since $f_3(x)$ saturates at 0.605 at high fields. For the case of strong spin–orbit scattering, the WL expression of equation (11) contributes the major negative contribution to the MC data. Moreover, the EEI expression of equation (8) makes a smaller, but also important negative contribution.

The MC data are predominantly negative for films on both sides of the MIT, with the exception of an anomalous behaviour that appears only at *small* magnetic fields below 0.4 T. The MC data for the metallic film No 16 are shown in figure 7, along with the theoretical fits made using equations (8) and (11). The fitting parameters are $D_{dif} =$
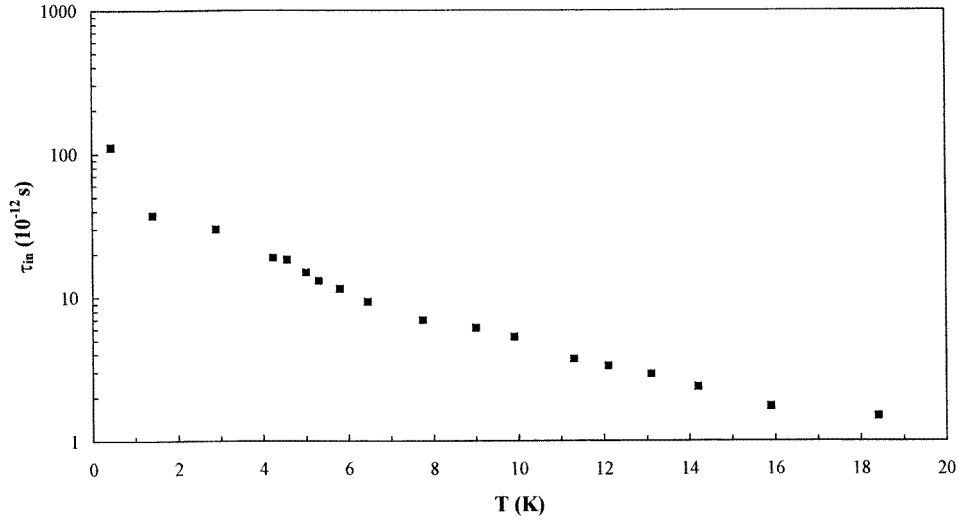
Figure 8. The inelastic scattering time versus temperature of the metallic film No 16, extracted from the MC data. The inelastic time follows a $T^{-1.2}$-law.

0.25 cm^2 s^{-1}, $\tilde{F}_\sigma = 0.20$, $B_{so} = 11.7$ T, using $Z_{Ni} = 28$ in $\tau_{so} = \tau_o (137/Z)^4$, $B_s = 0$ T, $B_{in}(T = 0.45$ K$) = 0.055$ T, $B_{in}(T = 1.41$ K$) = 0.18$ T, $B_{in}(T = 2.89$ K$) = 0.22$ T, and $B_{in}(T = 4.21$ K$) = 0.30$ T. There is strong spin–orbit scattering, producing a negative MC. The WL expression, equation (11), contributes 70% to the total negative MC magnitude owing to the strong spin–orbit field, while the EEI expression, equation (8), contributes the remaining 30%. Additional MC data up to 18.5 K yielded values for $B_{in}(T/K)$ which were then converted to inelastic scattering times $\tau_{in}(T/K)$ via $\tau_{in}(T/K) = \hbar/(4eD_{dif}B_{in})$. The results are illustrated in figure 8; above 4 K, the inelastic time follows a $\tau_{in}(T/K) \approx 7.5 \times 10^{-11} T^{-1.2}$ s dependence. The uncertainties in all of the fitting parameters are poor, about $\pm 100\%$.

In order to simplify the calculations, the magnetic scattering was taken to be very weak—that is, $B_s = 0$ or $\tau_s = \infty$. Bergmann has shown that moderately strong magnetic spin scattering broadens the MC curves by reducing the magnitudes by about 25% compared to those for films which have no magnetic impurities [40, 41]. In the extreme case of very strong magnetic spin scattering, Baxter *et al* have demonstrated that the negative MC arising from spin–orbit scattering is destroyed by magnetic impurity scattering [37]; this is surely not the case here. It is unlikely that Ni has a magnetic moment in amorphous nickel–silicon. There is recent evidence that very small clusters of Ni atoms are non-magnetic. From MC data taken on thin copper films deposited upon very small isolated Ni spheres of controlled diameter, Lin *et al* concluded that Ni spheres, having diameters smaller than 8 Å, possess no magnetic moment [42]. Beckmann and Bergmann also observed that pairs of Ni atoms have a magnetic moment, while single Ni atoms are non-magnetic [43, 44]. In our case, neglecting B_s is a second-order correction when compared to the uncertainties in D_{dif} and $\tilde{F}_\sigma$. According to the observations of Dynes' group [45], the presence of magnetic moments completely changes the nature of the electrical transport at low temperature, changing weakly localized metals into insulators.

The zero-field conductivity data for film No 16 can be fitted using the two zero-field expressions, equations (7) and (10), and the parameters determined from the MC fits. The
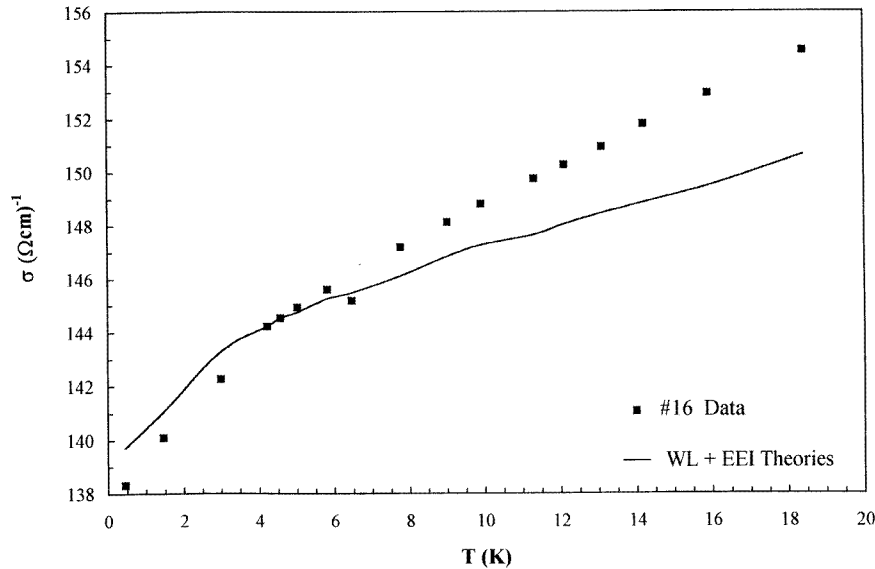
Figure 9. The zero-field conductivity of film No 16 versus temperature. The solid line is a fit based upon the 3D EEI and WL theories made using equations (7) and (10), and using the fitting parameters extracted from the MC data.

$\sigma(T)$ fit is of poor quality as shown in figure 9. In this case, the EEI expression contributes 85% to the total conductivity change with temperature, while the WL expression makes a small—15%—contribution. If just the EEI expression is used (equation (7)), neglecting the WL contribution of equation (10), the fit is good, as seen in figure 6; and the EEI contribution, $\sigma_{EEI} = 4.05T^{1/2}$ Ω^{-1} cm^{-1}, agrees extremely well with the empirical fit formula extracted from the data for film No 16 (table 2). However, the WL term cannot be neglected since it makes the major contribution to the negative MC data. Interestingly, the WL expression exhibits anti-localization below 10 K and localization above 10 K. When the WL expression, equation (10), is introduced, the fit is much poorer, as is clearly seen in figure 9; perhaps this expression is incorrect near the MIT or we have chosen an incorrect value for the spin–orbit scattering time. The small oscillations associated with the solid curve arise from the uncertainties in the inelastic scattering times deduced from the MC data.

When the MC data, evaluated both at the fixed reference temperature $T \approx 0.5$ K and at the fixed reference field $B \approx 3.45$ T, are plotted versus the Ni content x (using the EDAX results) for both metallic and insulating films, as seen in figure 10, the MC behaviour exhibits a negative maximum at 25 at.% Ni corresponding to film No 18; recall that, earlier, film No 18 was found to lie just above the MIT transition. Such a MC maximum has been reported previously by Abkemeier *et al* [3] and by Ovadyahu [46]. We suggest that the increasingly negative magnitudes of $\Delta\sigma$, as the MIT is approached from the metallic regime, result from the rapid decrease of the diffusion constant D_{dif} as $x \to x_c$; recall that the EEI MC expression, equation (8), scales inversely as $D_{dif}^{1/2}$. This effect would give rise to the negative increase of $\Delta\sigma$. We speculate that when the MIT is approached from above, the WL theory is no longer valid, and hence the contribution to the MC from the WL equation (11) rapidly falls to zero. Kleinert and Bryksin also predict that the WL theory
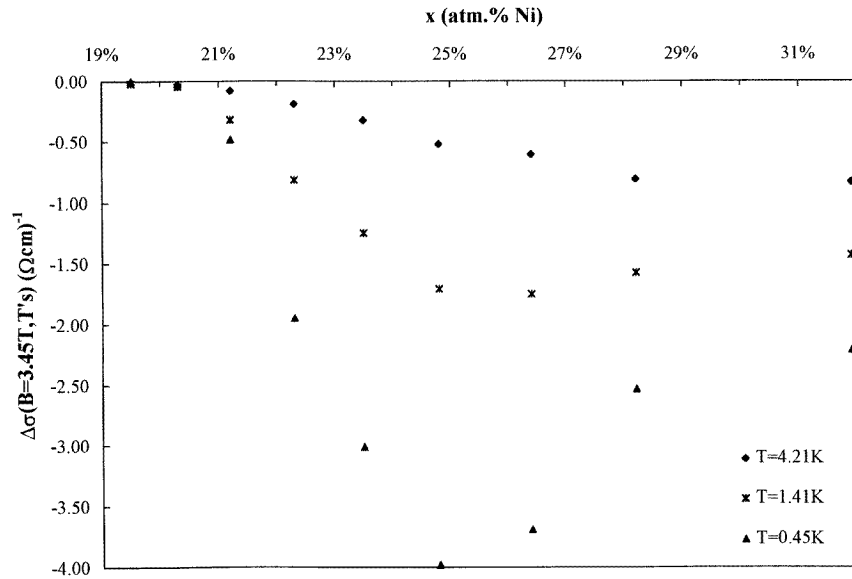
Figure 10. The magnetoconductance $\Delta\sigma(B = 3.45$ T, $T = 0.5$ K) versus Ni content x (based upon EDAX results) for both metallic and insulating films. The maximum in the negative MC data at $x_{max} \approx 25\%$ (film No 18) occurs at the MIT, also located at $x_c \approx 25\%$. A possible explanation for the negative maximum is given in the text. This behaviour could be used to identify the MIT in other amorphous systems.

breaks down at the MIT [47]. Hence a negative maximum in the MC is observed just before the MIT, followed by a decrease of the MC to zero below the MIT, since the EEI contribution is also depressed. Notice that in figure 10, at the highest temperature of 4.2 K, the negative MC peak disappears, since the contribution from the EEI term becomes very small owing to the strong dependence of g_3 upon temperature. This 'MC peak' should be a useful criterion for locating the MIT in other systems.

## 5. The low-field magnetoconductance data

All of the metallic films display an anomalous MC behaviour at temperatures below 1 K and at magnetic fields smaller than 0.35 T. For example, film No 16 exhibits a positive MC contribution as seen in figure 11. In the mK region at very small fields, there is also a negative MC spike; this negative MC contribution is not present in the MC data above 0.4 K. Interestingly, Heinrich *et al* have also observed this positive MC for amorphous Cr_xGe_{1-x} films [48]. The process might be associated with the formation of magnetic particles at the glass substrate–film interface [49].

6. The high-temperature conductivity data

All of the films exhibit conductivities that always decreased below room temperature, as seen in figure 2. To a very good approximation, the conductivities of the metallic films scale directly linearly with the temperature over the wide temperature interval of 30 K $< T <$ 300 K, as shown in figure 12. This linear temperature dependence of the
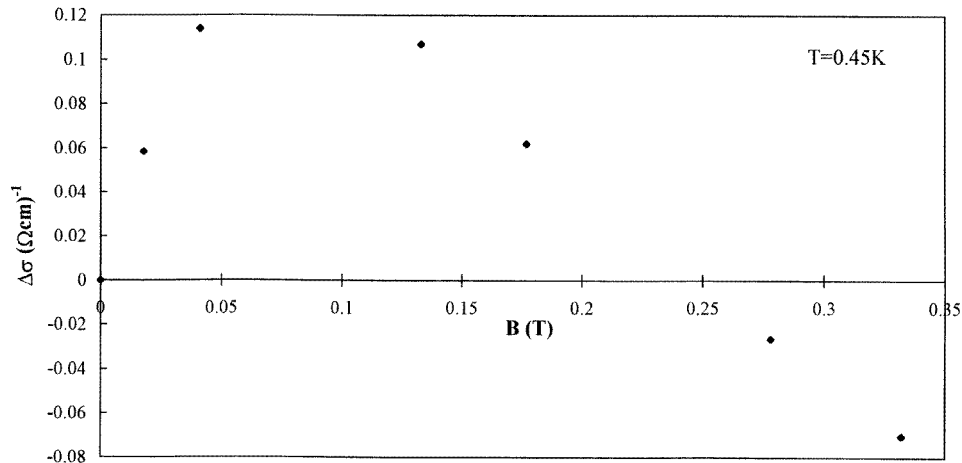
Figure 11. A plot of the low-field magnetoconductance behaviour of film No 16 versus small magnetic fields at $T = 0.45$ K.
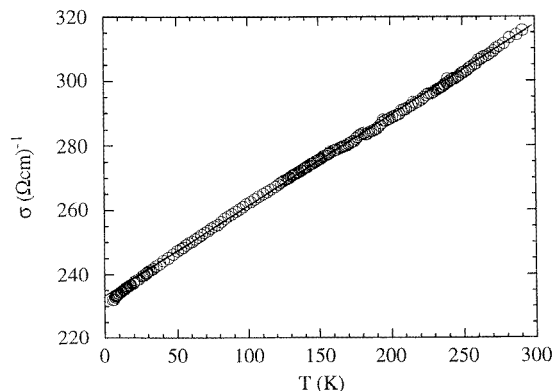
Figure 12. The zero-field conductivity versus T for the metallic film No 14. All of the metallic films exhibit conductivities that decrease *linearly* with temperature over this wide temperature interval.

conductivity has been observed by Dammer *et al* and also by Belu-Marian *et al* [1, 2]. The conductivity data can be fitted well over the entire temperature range using the expression $\sigma(T) = \sigma(0) + CT^{1/2} + AT^1$. Below 15 K, the conductivity closely follows a $T^{1/2}$-dependence according to the EEI theory. For film No 16 an acceptable empirical fit is given by $\sigma(T) = 135.8 + 3.70T^{1/2} + 0.177T^1$. Möbius was also able to fit the conductivity data for amorphous Cr_xSi_{1-x} with the above expression [50].

We are not aware of a fully satisfactory explanation for the linear term AT^1 in the metallic conductivity. One might be tempted to use the WL correction to the conductivity, namely equation (10) where $\sigma(T) \propto [D\tau_{in}(T/K)]^{-1/2}$. Tsuei has presented a convincing argument that the WL theory is valid even at room temperature for amorphous metals [51]. At liquid nitrogen temperatures and above, the inelastic scattering time should be dominated by electron–phonon scattering. According to Schmid, $\tau_{in}(T/K) \propto T^{-4}$ [52]; hence, one

would predict a quadratic temperature dependence rather than a linear dependence for $\sigma(T)$. However, this scattering time might not apply to amorphous solids. Below 50 K, phonon scattering should become negligible ($\Theta_D = 645$ K for Si) and electron–electron scattering should dominate. The Baber scattering expression can be used, where $\tau_{in}(T/K) \propto T^{-2}$ [53, 54]; this scattering expression yields the observed linear temperature dependence. It is not clear why this electron–electron scattering process should dominate over the electron–phonon scattering process above liquid nitrogen temperatures.

Acknowledgments

References

[1]   Dammer U, Adkins C J, Asal R and Davis E A 1993 *J. Non-Cryst. Solids* **164–166** 501
      Dammer U 1992 The metal–insulator transition in amorphous silicon–nickel alloys *MPhil Thesis* University of Cambridge
[2]   Belu-Marian A, Serbănescu, M D, Mănăilă R, Ivanov E, Malis O and Devenyi A 1995 *Thin Solid Films* **259** 105
[3]   Abkemeier K M, Adkins C J, Asal R and Davis E A 1992 *J. Phys.: Condens. Matter* **4** 9113
[4]   Abkemeier K M, Adkins C J, Asal R and Davis E A 1992 *Phil. Mag.* B **65** 675
[5]   Collver M M 1977 *Solid State Commun.* **23** 333
[6]   Collver M M 1978 *Appl. Phys. Lett.* **32** 574
[7]   Belu-Marian A, Serbănescu M D, Mănăilă R, Teodorescu V and Ivanov I 1994 *Thin Solid Films* **238** 312
[8]   Belu-Marian A, Serbănescu M D, Mănăilă R and Devenyi A 1995 *Appl. Surf. Sci.* **91** 63
[9]   Rosenbaum R, Heines A, Karpovskii M, Pilosof M and Witcomb M 1997 *J. Phys.: Condens. Matter* **9** 5413
[10] Sumanasekera G U, Williams B D, Baxter D V and Carini J P 1994 *Phys. Rev.* B **50** 2606
[11] Bergmann G 1996 private communications
[12] Möbius A 1996 private communications
      On the basis of Dresden RBS data on a Dresden series, Arnulf Möbius suggests rescaling the EDAX contents according to $x(\text{at.\% Ni, RBS}) = 0.884x(\text{at.\% Ni, EDAX}) - 2.26\%$. This amounts to a negative shift of about 6 at.% Ni of the EDAX values. Thus, the critical concentration x_c is bounded between 19% and 25% at.% Ni. In this paper, the absolute value of x_c is not required; only the distinction between the metallic and the insulating films is needed.
[13] Möbius A 1989 *Phys. Rev.* B **40** 4194
[14] Rosenbaum R L, Slutzky M, Möbius A and McLachlan D S 1994 *J. Phys.: Condens. Matter* **6** 7977
[15] Shoshany J, Goldner V, Rosenbaum R, Witcomb M, McLachlan D S, Palevski A, Karpovski M, Gladkikh A and Lereah Y 1996 *J. Phys.: Condens. Matter* **8** 1729
[16] Abrahams E, Anderson P W, Licciardello D C and Ramakrishnan T V 1979 *Phys. Rev. Lett.* **42** 693
[17] Mott N F 1972 *Phil. Mag.* **26** 1015
[18] Belitz D and Kirkpatrick T R 1994 *Rev. Mod. Phys.* **66** 322
[19] Nishida N, Furubayashi T, Yamaguchi M, Morigaki K and Ishimoto H 1985 *Solid State Electron.* **28** 81
[20] Yoshizumi S, Mael D, Geballe T H and Greene R L 1985 *Localization and Metal–Insulator Transitions* ed H Fritzsche and D Adler (New York: Plenum) p 81

Yoshizumi S, Mael D, Geballe T H and Greene R L 1985 *Localization and Metal–Insulator Transitions* ed
         H Fritzsche and D Adler (New York: Plenum) p 85
[21] Belitz D 1996 private communications
[22] Shlimak I, Kaveh M, Ussyshkin R, Ginodman V and Resnick L 1996 *Phys. Rev. Lett.* **77** 1103
[23] Entin-Wohlman O, Kapitulnik A, Alexander S and Deutscher G 1984 *Phys. Rev.* B **30** 2617
[24] Derrida B, Stauffer D, Herrmann H J and Vannimenus J 1983 *J. Physique Lett.* **44** L701
[25] Herrmann H J, Derrida B and Vannimenus J 1984 *Phys. Rev.* B **30** 4080
[26] Alexander S 1983 *Phys. Rev.* B **27** 1541
[27] Altshuler B L and Aronov A G 1983 *Solid State Commun.* **46** 429
[28] Newson D J and Pepper M 1986 *J. Phys. C: Solid State Phys.* **19** 3983
[29] Lee P A and Ramakrishnan T V 1985 *Rev. Mod. Phys.* **57** 308
[30] Feher G 1959 *Phys. Rev.* **114** 1219
[31] Roth L 1960 *Phys. Rev.* **118** 1531
[32] Ousset J C, Askenazy S, Rakoto H and Broto J M 1985 *J. Physique* **46** 2145
[33] Kawabata A 1980 *J. Phys. Soc. Japan* **49** 628
[34] Fukuyama H and Hoshino K 1981 *J. Phys. Soc. Japan* **50** 2131
[35] Hickey B J, Greig D and Howson M A 1987 *Phys. Rev.* B **36** 3074
[36] Bergmann G 1984 *Phys. Rep.* **107** 30
[37] Baxter D V, Richter R, Trudeau M L, Cochrane R W and Strom-Olsen J O 1989 *J. Physique* **50** 1673
[38] Abrikosov A A and Gor'kov L P 1962 *Zh. Eksp. Teor. Fiz.* **42** 1088 (Engl. Transl. 1962 *Sov. Phys.–JETP* **15**
         752)
[39] Meservey R and Tedrow P M 1978 *Phys. Rev. Lett.* **41** 805
[40] Bergmann G 1982 *Phys. Rev. Lett.* **49** 162
[41] Bergmann G and Mathon G 1985 *Solid State Commun.* **56** 881
[42] Lin J J, Jian W B, Yamada R and Kobayashi S 1996 *Int. Conf. on Electron Localization and Quantum
         Transport in Solids (Warsaw)* abstract booklet, p 135
[43] Beckmann H and Bergmann G 1996 *Phys. Rev.* B **54** 368
     Beckmann H and Bergmann G 1996 *Europhys. Lett.* **33** 563
[44] Bergmann G 1978 *Phys. Rev. Lett.* **41** 264
[45] Hellman F, Tran M Q, Gebala A E, Wilcox E M and Dynes R C 1996 *Phys. Rev. Lett.* **77** 4652
[46] Ovadyahu Z 1990 *Hopping and Related Phenomena* ed H Fritzsche and M Pollak (Singapore: World
         Scientific) p 195
[47] Kleinert P and Bryksin V V 1997 *Phys. Rev.* B **55** 1469
[48] Heinrich A, Vinzelberg H, Elefant D and Gladun C 1993 *J. Non-Cryst. Solids* **164–166** 513
[49] Zhang S 1992 *Appl. Phys. Lett.* **61** 1855
[50] Möbius A 1985 *J. Phys. C: Solid State Phys.* **18** 4639
[51] Tsuei C C 1986 *Phys. Rev. Lett.* **57** 1943
[52] Schmid A 1973 *Z. Phys.* **259** 421
[53] Baber W G 1937 *Proc. R. Soc.* **158** 383
[54] Ashcroft N W and Mermin N D 1976 *Solid State Physics* (Philadelphia, PA: Saunders College Publishing)
         p 346